Magnetic control of ultra-cold ^{6}Li and ^{174}Yb($^{3}P_{2}$) atom mixtures with Feshbach resonances

2015 New J. Phys. 17 045010

(http://iopscience.iop.org/1367-2630/17/4/045010)

New Journal of Physics
The open access journal at the forefront of physics

Deutsche Physikalische Gesellschaft DPG
IOP Institute of Physics

Published in partnership with: Deutsche Physikalische Gesellschaft and the Institute of Physics

OPEN ACCESS

RECEIVED
24 December 2014

REVISED
17 February 2015

ACCEPTED FOR PUBLICATION
19 March 2015

PUBLISHED
17 April 2015

PAPER

Magnetic control of ultra-cold ^{6}Li and ^{174}Yb($^{3}P_2$) atom mixtures with Feshbach resonances

Alexander Petrov[1,2], **Constantinos Makrides**[1] **and Svetlana Kotochigova**[1]

[1] Department of Physics, Temple University, Philadelphia, PA 19122, USA
[2] Alternative address: NRC "Kurchatov Institute" PNPI, 188300; Division of Quantum Mechanics, St. Petersburg State University, 198904, Russia

E-mail: skotoch@temple.edu

Keywords: high-spin atomic system, Feshbach resonances, mata-stable states, magnetic photoassociation, close-coupling method

Abstract

We theoretically evaluate the feasibility to form magnetically-tunable Feshbach molecules in collisions between fermionic ^{6}Li atoms and bosonic metastable ^{174}Yb($^{3}P_2$) atoms. In contrast to the well-studied alkali-metal atom collisions, collisions with meta-stable atoms are highly anisotropic. Our first-principle coupled-channel calculation of these collisions reveals the existence of broad Feshbach resonances due to the combined effect of anisotropic-molecular and atomic–hyperfine interactions. In order to fit our predictions to the specific positions of experimentally-observed broad resonance structures (Dowd *et al* 2014) we optimized the shape of the short-range potentials by direct least-square fitting. This allowed us to identify the dominant resonance by its leading angular momentum quantum numbers and describe the role of collisional anisotropy in the creation and broadening of this and other resonances.

The formation of ultracold molecules with a single unpaired electron allowing for coupling of the electron spin with the rotational angular momentum of the molecule has received increasing interest [2–4]. For example, the authors in [2] proposed that such spin-rotational splitting of $^{2}\Sigma^{+}$ molecular rotational states can make the long-range electric dipole–dipole interaction between molecules spin-dependent. Then, these molecules confined in two-dimensional optical lattices create a class of ultracold molecules that can realize spin-lattice models with unique topological properties.

Ultracold $^{2}\Sigma^{+}$ molecules can be formed from an alkali-metal and an alkaline-earth-like atom in the ground or even long-lived metastable states. Experimental efforts toward production of these ground-state molecules are in their initial stages [1, 5–9]. The success of these experiments significantly depends on the realization of a two-step process, when a mixed quantum gas of alkali-metal and alkaline-earth-like atoms is first optically associated into weakly-bound molecules, which are then transferred into the rovibrational ground state.

Photoassociation for homonuclear alkaline-earth-like molecules via so-called optical Feshbach tuning was pioneered by [10–12]. This photoassociative tuning becomes possible due to the existence of long-lived excited molecular states near the narrow intercombination lines of the alkaline-earth-like atoms. Recent successful experiments [13–16] showed that a two-photon optical Feshbach resonance can be used to couple two colliding atoms to a vibrational level of the molecular ground state. The suppressed excited-state spontaneous decay makes efficient coherent molecular formation possible.

An alternative method to form ultracold molecules from ultracold atoms is by magneto-association. Magnetic Feshbach resonances have had an enormous impact on the field of laser-cooled ultra-cold atoms and molecules [17–21]. These resonances have allowed a tunable, variable interaction strength by simply varying the strength of an external magnetic field (typically on the order of 100 G or 10 mT). They are now widely used to investigate Efimov physics [22], create ultracold molecular gasses [19, 23], and to simulate unique many-body phases [24]. So far, these resonances have been restricted to systems with ground-state alkali-metal and ground-state rare-earth species [20, 25–29]. Only recently have experiments searching for resonances in collisions with

electronic excited atoms sprung up. [1, 30] detected the first resonances between ultra-cold ground state Yb or Li and excited Yb * in the metastable $^3P_2$ state.

The nature of Feshbach resonances in alkali and alkaline-earth-like atomic collisions significantly differs from that in alkali-metal atom collisions. In alkali metals the hyperfine interaction between electron and nuclear spins gives sufficient complexity that leads to the appearance of Feshbach resonances. In alkaline-earth-like atoms such hyperfine interaction does not exist as the nuclear spin is decoupled from the electronic degree of freedom. Nevertheless, [31, 32] showed that magnetically tunable Feshbach resonances in such systems can occur and are due to a weak R-dependent behavior of the hyperfine coupling constant of the alkali-metal atom, where R is the interatomic separation between the atoms. These resonances are predicted to be narrow, on the order of mG, and most likely appear at large magnetic field strengths. Hence, they are difficult to observe and control.

An interesting approach to induce and modify the position and width of narrow Feshbach resonances was proposed in [33]. The authors show that intense nonresonant radiation can increase the resonance widths by three orders of magnitude up to a few Gauss. These ac-field-induced resonances can be used for the production of ultra-cold ground state molecules from the colliding atoms. In addition, [34–36] suggested to apply an external dc-electric field with or without a magnetic field to control the interaction between ultra-cold atoms.

Another promising way to observe broader and stronger magnetic Feshbach resonances and subject of this study is to consider interactions between one ground and one long-lived metastable atom. These metastable Feshbach resonances and its associated weakly-bound metastable molecule might be used to efficiently transfer colliding atoms to a vibrational level of the absolute molecular ground state.

We report on widening the search for Feshbach resonances in these exotic collisions by investigating heteronuclear collisions of ground-state alkali-metal ^{6}Li and long-lived metastable rare-earth ^{174}Yb atoms. We demonstrate that the existence of magnetically-tunable Feshbach molecules for this system leads to formation of broad and strong resonances. Furthermore, we show that the origin of these Feshbach resonances is the result of a combination of exchange interactions and scattering anisotropies, where the interactions depend on the orientation of the interatomic axis relative to the magnetic field direction. The broad magnetic Feshbach resonances have non-zero orbital angular momentum $\vec{\ell}$.

Our results confirm earlier predictions by [37] that resonances are strongly suppressed due to inelastic processes to energetically lower-lying $^3P_1$ and $^3P_0$ states. Nevertheless, a recent experiment [1] on the ^{6}Li+^{174}Yb ($^3P_2$) system has shown that resonances exists. Here, we have performed least-square simulations on the shape of the molecular potentials and reproduced their resonance spectrum. In addition, we identified the strongest and dominant resonance in terms of its mixture of partial waves ℓ.

1. Interaction potentials

For the determination of collisional properties of Li($^2S_{1/2}$) + Yb($^3P_2$) system we have (i) determined the short-range and long-range electronic interaction potentials $V(\vec{R}, \tau)$ and (ii) setup a close-coupling calculation that treats the hyperfine and Zeeman interaction, molecular rotation, magnetic dipole–dipole (MDD) interaction, and the electronic interactions on equal footing. Here, $\vec{R}$ describes the interatomic separation and orientation and τ labels other quantum numbers that uniquely label the electronic potentials. We have calculated the non-relativistic doublet $^2\Sigma^+$ and $^2\Pi$ and quartet $^4\Sigma^+$ and $^4\Pi$ potentials, shown in figure 1, using the configuration-interaction method within the MolPro package [38].

We used the aug-cc-pCVTZ basis set for Li [39] and chose a basis set constructed from the (15s 14p 12d 11f 8g)/(8s 8p 7d 7f 5g) wave functions of Dolg and Cao [40, 41] for Yb. The ytterbium basis relies on a relativistic pseudopotential that describes the inner orbitals up to the $3d^{10}$ shell. Only, the 2s valence electrons of Li and $4f^{10}$ and $6s^2$ valence electrons of Yb are correlated in the *ab initio* calculation. Our potentials agree well with the calculations of [42]. However, the potentials are not spectroscopically accurate and we have modified their shape to fit to the experimental loss rate spectrum. For $R > 27a_0$, beyond the Le Roy radius where the electron clouds of the atoms have negligible overlap, these electronic potentials are smoothly connected to the long-range isotropic and anisotropic van-der-Waals potentials determined from atomic polarizabilities [9]. In addition, we included the MDD interaction.

2. Relative strength of various interactions

Next, we find it instructive to analyze the relative strength of the long-range atom–atom interactions with the Zeeman, hyperfine, and relative rotational interactions. Figure 2 shows the two major anisotropic interactions, the MDD C_3/R^3 and the anisotropic dispersion $\Delta C_6/R^6$ (AD) interaction, which can lead to the reorientation of

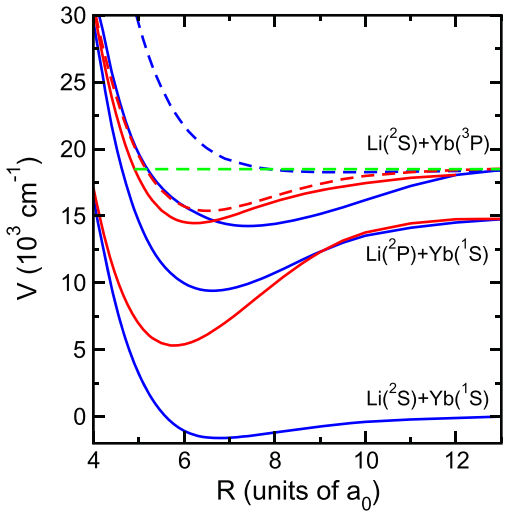

Figure 1. The ground and lowest excited non-relativistic potentials of the LiYb molecule as a function of internuclear separation R. Here a_0 is the Bohr radius of 0.0529 nm. Solid blue and red curves are $^2\Sigma^+$ and $^2\Pi$ potentials, while dashed blue and red curves are $^4\Sigma^+$ and $^4\Pi$ potentials, respectively. Four metastable potentials dissociate to the Li(^{2}S$_{1/2}$)+Yb(^{3}P) limit and are used in our coupled-channel modeling. The green dashed horizontal line indicates the energy of a Feshbach molecule near the ^{2}S+^{3}P limit.

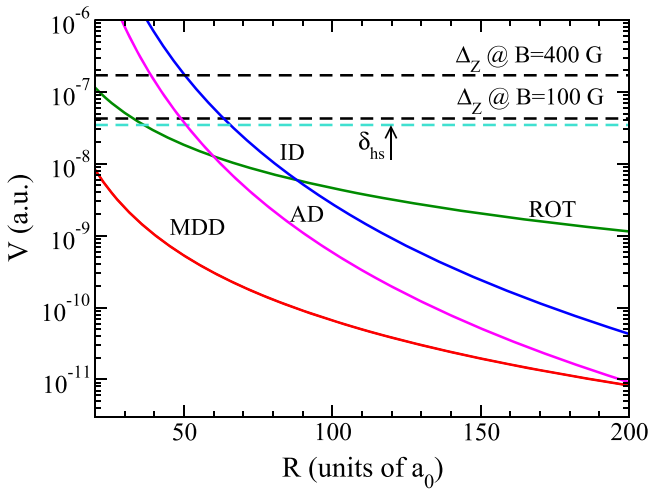

Figure 2. Level splitting due to the dominant interactions between ^{6}Li and Yb(^{3}P) as a function of interatomic separation. Here Δ_Z is the Zeeman splitting at two magnetic fields, $\delta_{\rm hs}$ is hyperfine splitting of ground state ^{6}Li, MDD is the magnetic dipole–dipole interaction C_3/R^3, ID is the isotropic dispersion interaction C_6/R^6, and AD is an estimate of anisotropic dispersion interaction $\Delta C_6/R^6$. Finally, ROT is the rotational energy $\hbar^2/(2\mu R^2)$. We used $C_6 = 2694E_h a_0^6$, $\Delta C_6 = 242E_h a_0^6$, and $C_3 = 6.6 \times 10^{-5}E_h a_0^3$. Here $E_h = 4.3610^{-18}$ J is the Hartree.

the Li and Yb * angular momenta during a collision, as a function of R. These potentials as well as the isotropic dispersion C_6/R^6 (ID) interaction were drawn, assuming weighted-average values of C_3 and C_6, and ΔC_6, based on our previous calculations [9]. In fact, $C_6 = (C_{6\Sigma} + 2C_{6\Pi})/3$, where $C_{6\Sigma}$ and $C_{6\Sigma}$ are the dispersion coefficient of the Σ and Π potentials, respectively. The ΔC_6 coefficient is found from tensor analyses of the parallel and perpendicular components of the dynamic polarizability, as described in section 2 of [43]. In addition, the molecule can rotate, here estimated by $\hbar^2/(2\mu R^2)$ with reduced mass μ. Finally, hyperfine splitting (hs) of the ^{6}Li atom, and the Zeeman interaction at magnetic field strengths $B = 100$ and 400 G are shown. At much shorter separation and larger energies, not shown in the figure, the exchange interaction due to the exponentially-increasing electron cloud overlap lifts the degeneracy of the double and quartet potentials and mixes the spin–orbit states of the Yb(^{3}P$_j$) levels.

The figure is most easily interpreted in the coordinate system and angular-momentum basis set with projection quantum numbers defined along the external magnetic field direction. In this coordinate system the rotational, spin–orbit, and hyperfine, and Zeeman interactions as well as the ID potential shift molecular levels, whereas the exchange interaction, the MDD interaction, and the anisotropic component of the dispersion

potential lead to coupling between rotational, hyperfine, and Zeeman components. For different interatomic separations different forces dominate. For example, when the curves for the magnetic dipole or AD interaction cross the hyperfine, Zeeman and/or rotational energies spin flips combined with changes in the rotational state can occur. In fact, the AD curve crosses the $B = 100$ and 400 G Zeeman curves near $R = 50a_0$ and $40a_0$, respectively, whereas the MDD curve crosses $\delta_{\rm hs}$ and Δ_Z at much shorter R, where chemical bonding or exchange interaction will also play an important role.

3. Close-coupling calculation

We have setup a close-coupling model for the scattering of fermionic ^{6}Li and the metastable bosonic ^{174}Yb isotope. The lithium atom is uniquely specified by electron spin $s_{\rm Li} = 1/2$ and nuclear spin $i_{\rm Li} = 1$. The metastable Yb* is specified by electron spin $s_{\rm Yb} = 1$ and electron orbital angular momentum $l_{\rm Yb} = 1$. It is also convenient to define total atomic angular momenta $\vec{f}_{\rm Li} = \vec{s}_{\rm Li} + \vec{i}_{\rm Li}$ and $\vec{j}_{\rm Yb} = \vec{s}_{\rm Yb} + \vec{l}_{\rm Yb}$ for Li and Yb*, respectively. Their projections along the B-field direction are $m_{\rm Li}$ and $m_{\rm Yb}$. The Hamiltonian for the relative motion of the two such atoms in a magnetic field B along the $\hat{z}$ direction is

$$H = -\frac{\hbar^2}{2\mu_r}\frac{{\rm d}^2}{{\rm d}R^2} + \frac{\vec{\ell}^{\,2}}{2\mu_r R^2} + H_{\rm SO} + H_{\rm hf} + H_Z + U\left(\vec{R}\right), \qquad (1)$$

where the rotational Hamiltonian is $\hbar^2\vec{\ell}^{\,2}/(2\mu R^2)$, the spin–orbit interaction of Yb* is $H_{\rm SO} = a_{\rm SO}\vec{l}_{\rm Yb}\cdot\vec{s}_{\rm Yb}$, the hyperfine interaction of ^{6}Li is $H_{\rm hf} = a_{\rm hf}\vec{s}_{\rm Li}\cdot\vec{i}_{\rm Li}$, and the Zeeman interaction $H_Z = (g_{e,{\rm Li}}s_{{\rm Li},z} + g_{N,{\rm Li}}i_{{\rm Li},z} + l_{{\rm Yb},z} + g_{e,{\rm Yb}}s_{{\rm Yb},z})\mu_B B$, with Bohr magneton μ_B and projection operators $s_{{\rm Li},z}$ etc. The strengths $a_{\rm SO}$ and $a_{\rm hf}$ are taken from [44, 45]. The $g_{e,{\rm Li}}$, $g_{e,{\rm Yb}}$, and $g_{N,{\rm Li}}$ are the electronic and nuclear g-factors of Li and Yb* from [45, 46]. Finally, $U(\vec{R})$ describes the MDD interaction and the non-relativistic electronic potentials, which are reexpressed in terms of (tensor) coupling operators between electron spins $\vec{s}_{\rm Li}$ and $\vec{s}_{\rm Yb}$, and the angular momenta $\vec{l}_{\rm Yb}$ and $\vec{\ell}$. For $R \to \infty$ the interaction $U(\vec{R}) \to 0$.

There are four contributions to $U(\vec{R})$: a spin-independent isotropic potential $V_{\rm iso}(R)$, which is proportional to an attractive $1/R^6$ potential for large separations, a short-range isotropic exchange interaction $V_{\rm exc}^{\Sigma,\Pi}(R)[\vec{s}_{\rm Li}\bigotimes\vec{s}_{\rm Yb}]_{00} = -V_{\rm exc}^{\Sigma,\Pi}(R)\vec{s}_{\rm Li}\cdot\vec{s}_{\rm Yb}/\sqrt{3}$, which splits doublet from quartet Σ and Π potentials and falls of exponentially for large R, and an anisotropic quadrupole-like interaction $V_{\rm ani}(R)[\hat{C}_2(\hat{R})\bigotimes[\vec{l}_{\rm Yb}\bigotimes\vec{l}_{\rm Yb}]_2]_{00}$, which lifts the degeneracy of the Σ and Π potentials and $V_{\rm ani}(R) \propto 1/R^6$ for large R. Here, $\hat{C}_{kq}(\hat{R})$ is a spherical harmonic. The four interaction strengths $V_{\rm iso}(R)$, $V_{\rm exc}^{\Sigma,\Pi}(R)$, and $V_{\rm ani}(R)$ are constructed such that in the body-fixed frame with projections along the internuclear axis the sum of the interactions closely reproduces our four non-relativistic potentials.

The Hamiltonian is constructed in the atomic basis or channels $Y_{\ell m_\ell}(\theta,\,\phi)|\alpha_{\rm Li}\rangle|\alpha_{\rm Yb}\rangle$, where $Y_{\ell m_\ell}(\theta,\,\phi)$ is a spherical harmonic and angles θ and ϕ give the orientation of the internuclear axis relative to the magnetic field direction. Hence, the rotational Hamiltonian is diagonal in this basis. The kets $|\alpha_{\rm Li}\rangle$ are eigen states of the atomic Zeeman plus hyperfine Hamiltonian of ^{6}Li. For fields $B > 100$ G, of interest in this paper and where the Paschen–Back limit holds, we denote states by $\alpha_{\rm Li} = m_s,\, m_i$, where m_s and m_i are the projections of $\vec{s}_{\rm Li}$ and $\vec{i}_{\rm Li}$, respectively (and $m_{\rm Li} = m_s + m_i$). The kets $|\alpha_{\rm Yb}\rangle$ are eigen states of the atomic spin–orbit and Zeeman Hamiltonian of ^{174}Yb in the ^{3}P term. As the spin–orbit interaction is orders of magnitude larger than the Zeeman interaction we denote the states by $\alpha_{\rm Yb} = j_{\rm Yb}\,m_{\rm Yb}$. Coupling between the basis states is due to $U(\vec{R},\,\tau)$. The Hamiltonian conserves $M_{\rm tot} = m_{\rm Li} + m_{\rm Yb} + m_\ell$ and only even (odd) ℓ are coupled.

In the experiment of [1] the ^{6}Li atoms are prepared in the energetically-lowest hyperfine state with $m_{\rm Li} = 1/2$ while the Yb atoms are prepared in the $^3{\rm P}_2$ ($|j_{\rm Yb}\,m_{\rm Yb}\rangle = |2,\,-1\rangle$) sublevel. For ultra-cold gasses with temperatures near 1 μK we can focus on so-called s-wave or $\ell = 0$ scattering. Theoretically, this corresponds to calculations including channels with $M_{\rm tot} = -1/2$ and even partial waves ℓ. We will also present results for ultra-cold scattering with Yb* prepared in the state $|j_{\rm Yb}\,m_{\rm Yb}\rangle = |2,\,-2\rangle$. This corresponds to calculations for $M_{\rm tot} = -3/2$.

Figure 3 shows a sample of the medium- to long-range adiabatic potentials, obtained by diagonalizing H excluding the radial kinetic energy operator, as a function of interatomic separation R near the Yb*($^3{\rm P}_2$) dissociation limit at a magnetic field of $B = 300$ G. Only potentials dissociating to the $f_{\rm Li} = 1/2$ or 3/2 and $j_{\rm Yb} = 2$, $m_{\rm Yb} = 0,\,-1,\,-2$ limits are visible in the figure. Inelastic collisional losses to energetically lower-lying Yb*(^{3}P, $j_{\rm Yb} = 0,\,1$) states do nevertheless exist. Feshbach resonances occur in channels with a dissociation energy above that of the entrance channel.

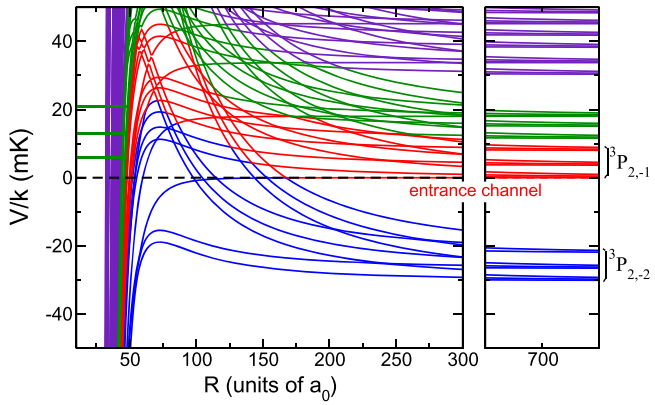

Figure 3. Adiabatic potentials of colliding ^{6}Li(^{2}S$_{1/2}$) and ^{174}Yb(^{3}P) near the ^{3}P$_2$ dissociation limit at a magnetic field of $B = 300$ G and $M_{\rm tot} = -1/2$ as a function of interatomic separation R. Channels with even partial wave ℓ up to 6 are included. Curves approaching the same dissociation limit correspond to different partial waves. The collision starts in the s-wave $m_{\rm Li} = 1/2$ and $j_{\rm Yb} = 2$, $m_{\rm Yb} = -1$ channel indicated by the dashed horizontal line. A resonance occur when the energy a bound state of a closed channel, which are schematically shown as dark-green horizontal solid lines close to the entrance-channel energy. Here $k = 1.38065 \times 10^{-23}$ J K^{-1} is the Boltzmann constant.

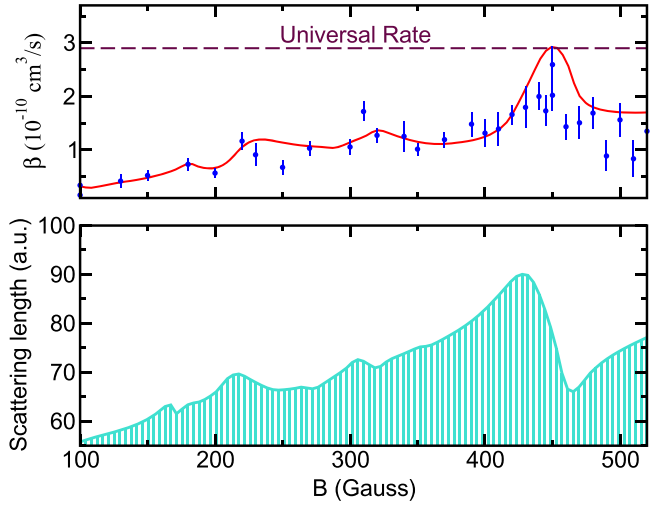

Figure 4. Upper panel: loss rate coefficient in the ^{6}Li ($m_s = -1/2$, $m_i = 1$)+^{174}Yb (^{3}P$_2$, $j = 2$, $m = -1$) collision as a function of magnetic field B. The experimental data (blue dots with one standard-deviation uncertainties) is obtained at a temperature of $T = 1.6$ μK. The theoretical simulation (solid red curve) with optimized short-range potentials is obtained for the same temperature. Lower panel: scattering length as a function of B at collision energy $E/k = 1.6$ μK. The short-range potentials are as the same as for the rate in upper panel. Two dashed line indicates the van der Waals length with average value of $C_6 = 2694$ a.u..

Figure 4 shows the experimental inelastic rate coefficient [1] at a temperature of 1.6 μK in the collision between ^{6}Li and ^{174} Yb* atoms and our best-fit theoretical inelastic rate coefficient at a collision energy of $E/k = 1.6$ μK. We include channels with $M_{\rm tot} = -1/2$ and even ℓ up to 8 leading to a close-coupling calculation with 99 channels. A thermal average of the theoretical inelastic rate coefficient is not required as we are in the Wigner threshold limit where this rate is independent of collision energy. We observe at least one clear resonance at $B = 450$ G and possibly three weaker resonances. From calculations that include fewer partial waves we find that the resonances can not be labeled by a single partial wave. Their locations shift significantly and only converge to within a few Gauss when $\ell = 8$ channels are included. Including channels with $\ell \leqslant 10$ shifts resonance by no more than 0.1 G. This is well within the width of the resonances for both figures 4 and 5. Consequently, we conclude that it is sufficient to include channels up to $\ell \leqslant 8$.

Our bound-state calculation allows us to identify the dominant closed channel that couples to the s-wave entrance channel at $B = 450$ G. We identify this channel with the $\ell = 4$ partial wave and projection $m_\ell = 1$. This coupling is due to anisotropic interactions, such as the AD forces at large separations. Moreover, this channel dissociates to the atomic limit ^{6}Li($m_s = 1/2, m_i = -1$) + ^{174}Yb(^{3}P, $j = 2, m = -1$), which lies above the entrance channel (see figure 3).

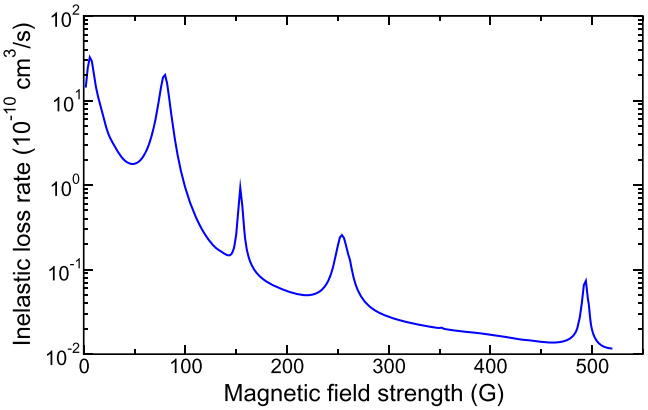

Figure 5. Predicted theoretical loss rate coefficient in the ^{6}Li ($m_s = 1/2$, $m_i = -1$)+^{174}Yb (^{3}P$_2$, $j_{\rm Yb} = 2$, $m_{\rm Yb} = -2$) collision with $M_{\rm tot} = -3/2$ and collision energy of $E/k = 1.6$ μK as a function of magnetic field B. The simulation is performed with optimized short-range potentials as in figure 4.

Figure 4 also provides evidence that the inelastic rate of the strong resonance is close to the universal rate, as shown by the dashed line in figure 4. This is a clear indication that the collisional system is close to the universal regime for losses on the dominant resonance and lies well below for other magnetic fields [43, 47].

The agreement between the experimental [1] and our theoretical spectrum is only obtained by allowing the coefficients $V_{\rm iso}(R)$, $V_{\rm exc}^{\Sigma,\Pi}(R)$, and $V_{\rm ani}(R)$ to vary such that the depth of the four non-relativistic potential curves is changed. We can not exclude the existence of other shapes of potentials which will lead to a loss rates that is consistent with the experimental data.

The lower panel of figure 4 shows the scattering length a as a function of the magnetic field strength for the collisions between ^{6}Li ($m_s = -1/2$, $m_i = 1$) and ^{174}Yb (^{3}P$_2$, $j_{\rm Yb} = 2$, $m_{\rm Yb} = -1$) atoms at a collisional energy of 1.6 μK. Here the scattering length is defined through $S_{\rm elastic} = \exp(-2ik[a - ib])$, where $S_{\rm elastic}$ is the elastic S-matrix element for the s-wave scattering channel, wavenumber k is given by $E = \hbar^2k^2/(2\mu)$, and positive length b can be related to the inelastic loss rate coefficient. The resonance features of a correspond to those for the inelastic rate in figure 4. The Feshbach resonance centered at 450 G has a well resolved Fano profile with a background value close to $75a_0$.

We have also studied the role of the Yb spin–orbit interaction and anisotropy of the electronic potentials on the Feshbach resonance structure. Our analyses indicate that for most magnetic fields the resonance features are broadened by the losses energetically lower collision channels with non-zero orbital angular momentum ℓ. This confirmes our predictions about the importance of anisotropic coupling between the short-range potentials. Moreover, we also observe that, except for small fields, more than one half of the loss goes into ^{3}P$_2$, $j = 2$, $m = -2$ channels. In addition, a significant fraction of the population ends up in the Yb(^{3}P$_1$) spin–orbit state (see figure 4(b) in [1]).

4. Conclusion

We discussed advances in the understanding of scattering properties of high-spin open-shell atomic systems. In particular, our attention was directed towards collisions between fermionic lithium atoms in their absolute ground state with bosonic ytterbium in its meta-stable ^{3}P$_2$ state. Both species, either with their bosonic or fermionic isotopes, have been successfully cooled to quantum degeneracy and confined in optical dipole traps or optical lattices, allowing the study of their collisions at the quantum level. We observed magnetic Feshbach resonances in collisions with the meta-stable ^{174}Yb atoms even though this atom was prepared in the $m_{\rm Yb} = -1$ magnetic sub level, which is not the energetically-lowest ^{3}P$_2$ Zeeman state. With couple-channels calculations we have elucidated the role of anisotropies in the creation of these resonances and by optimizing the shape of the short-range potentials reproduced the measured loss rate for magnetic fields up to 500 G.

Initially, collisions between ground state Li and metastable Yb in the ^{3}P$_2$ state seemed to be a good system in which to form strong Feshbach resonances, since the Yb life time is 15s and interactions with Li atoms is highly anisotropic. Our calculations, however, show that when Yb atoms are not prepared in the energetically-lowest magnetic sublevel the resonances have large inelastic losses (on the order of 10^{-10} cm^3 s^{-1}). This large rate coefficient might be an obstacle to use them in stimulated Raman adiabatic passage schemes to create the ground state molecules. On the other hand, we also found that inelastic loss for the resonances in collisions with the

energetically-lowest magnetic sublevel of Yb is an order of magnitude smaller. These resonances if experimentally confirmed can be promising candidates for Raman transfer. In figure 5 we present a prediction for the Feshbach spectrum for the collision between ^{6}Li and ^{174}Yb ($^3P_2$, $j = 2$, $m = -2$) based on the optimized potentials.

Acknowledgments

This work is supported by the AFOSR grant No. FA9550-14-1-0321, the ARO MURI grant No. W911NF-12-1-0476, and the NSF grant No. PHY-1308573.

References

[1] Dowd W, Roy R J, Shrestha R K, Petrov A, Makrides C, Kotochigova S and Gupta S 2015 *New J. Phys.* (accepted)
[2] Micheli A, Brennen G K and Zoller P 2006 *Nat. Phys.* **2** 341
[3] Carr L D, DeMille D, Krems R and Ye J 2009 *New J. Phys.* **11** 055049
[4] Perez-Rios J, Herrera F and Krems R V 2010 *New J. Phys.* **12** 103007
[5] Okava M, Hara H, Muramatsu M, Doi K, Uetake S, Takasu Y and Takahashi Y 2010 *Appl. Phys.* B **98** 691
[6] Nemitz N, Baumer F, Münchow F, Tassy S and Görlitz A 2009 *Phys. Rev.* A **79** 061403
[7] Ivanov V V, Khramov A, Hansen A H, Dowd W H, Munchow F, Jamison A O and Gupta S 2011 *Phys. Rev. Lett.* **106** 153201
[8] Hara H, Takasu Y, Yamaoka Y, Doyle J M and Takahashi Y 2011 *Phys. Rev. Lett.* **106** 205304
[9] Khramov A, Hansen A, Dowd W, Roy R J, Makrides C, Petrov A, Kotochigova S and Gupta S 2014 *Phys. Rev. Lett.* **112** 033201
[10] Ciurylo R, Tiesinga E and Julienne P S 2005 *Phys. Rev.* A **71** 030701
[11] Jones K M, Tiesinga E, Lett P D and Julienne P S 2006 *Rev. Mod. Phys.* **78** 483
[12] Enomoto K, Kasa K, Kitagawa M and Takahashi Y 2008 *Phys. Rev. Lett.* **101** 203201
[13] Yamazaki R, Taie S, Sugawa S and Takahashi Y 2010 *Phys. Rev. Lett.* **105** 050405
[14] Blatt S, Nicholson T L, Bloom B J, Willams J R, Thosen J W, Julienne P S and Ye J 2011 *Phys. Rev. Lett.* **107** 073202
[15] Yan M, DeSalvo B J, Ramachandhran B, Pu H and Killian T C 2013 *Phys. Rev. Lett.* **110** 123201
[16] Yamazaki R, Taie S, Sugawa S, Enomoto K and Takahashi Y 2013 *Phys. Rev.* A **87** 010704
[17] Tiesinga E, Verhaar B J and Stoof H T C 1993 *Phys. Rev.* A **47** 4114
[18] Inouye S, Andrews M R, Stenger J, Miesner H-J, Stamper-Kurn D M and Ketterle W 1998 *Nature* **392** 151
[19] Köhler T, Góral K and Julienne P 2006 *Rev. Mod. Phys.* **78** 1311
[20] Chin C, Grimm R, Julienne P S and Tiesinga E 2010 *Rev. Mod. Phys.* **82** 1225
[21] Kotochigova S 2014 *Rep. Prog. Phys.* **77** 093901
[22] Kraemer T *et al* 2006 *Nature* **440** 315
[23] Ni K-K, Ospelkaus S, de Miranda M H G, Pe'er A, Neyenhuis B, Zirbel J J, Kotochigova S, Julienne P S, Jin D S and Ye J 2008 *Science* **322** 231
[24] Bloch I, Dalibard J and Zwerger W 2008 *Rev. Mod. Phys.* **80** 885
[25] Werner J, Griesmaier A, Hensler S, Stuhler J, Pfau T, Simoni A and Tiesinga E 2005 *Phys. Rev. Lett.* **94** 183201
[26] Petrov A, Tiesinga E and Kotochigova S 2012 *Phys. Rev. Lett.* **109** 103002
[27] Baumann K, Burdick N Q, Lu M and Lev B L 2014 *Phys. Rev.* A **89** 020701
[28] Aikawa K, Frisch A, Mark M, Baier S, Rietzler A, Grimm R and Ferlaino F 2012 *Phys. Rev. Lett.* **108** 210401
[29] Frisch A, Mark M, Aikawa K, Ferlaino F, Bohn J L, Makrides C, Petrov A and Kotochigova S 2014 *Nature* **507** 475
[30] Kato S, Sugawa S, Shibata K, Yamamoto R and Takahashi Y 2013 *Phys. Rev. Lett.* **110** 173201
[31] Żuchowski P S, Aldegunde J and Hutson J M 2010 *Phys. Rev. Lett.* **105** 153201
[32] Brue D and Hutson J M 2012 *Phys. Rev. Lett.* **108** 043201
[33] Tomza M, González-Férez R, Koch C P and Moszynski R 2014 *Phys. Rev. Lett.* **112** 113201
[34] Marcelis B, Verhaar B and Kokkelmans S 2008 *Phys. Rev. Lett.* **100** 153201
[35] Li Z and Krems R V 2007 *Phys. Rev.* A **75** 032709
[36] Krems R V 2006 *Phys. Rev. Lett.* **96** 123202
[37] Gonzalez-Martinez M L and Hutson J M 2013 *Phys. Rev.* A **88** 020701
[38] Werner H-J, Knowles P J, Knizia G, Manby F R and Schütz M 2012 *Comput. Mol. Sci.* **2** 242
[39] Prascher B P, Woon D E, Peterson K A, Dunning T H and Wilson A K 2011 *Theor. Chem. Acc.* **128** 69
[40] Cao X and Dolg M 2001 *J. Chem. Phys.* **115** 7348
[41] Dolg M 2013 private communication
[42] Gopakumar G, Abe M, Das B P, Hara M and Hirao K 2010 *J. Chem. Phys.* **133** 124317
[43] Kotochigova S 2010 *New J. Phys.* **12** 073041
[44] Meggers W F and Tech J L 1978 *J. Res. Natl Bur. Stand.* **83** 13
[45] Arimondo E, Inguscio M and Violino P 1977 *Rev. Mod. Phys.* **49** 31
[46] Kramida A, Ralchenko Y, Reader J and Team N A 2014 *NIST Atomic Spectra Database (ver. 5.0)* http://physics.nist.gov/asd
[47] Idziaszek Z and Julienne P S 2010 *Phys. Rev. Lett.* **104** 113202